Hindawi
Advances in Materials Science and Engineering
Volume 2022, Article ID 3274672, 16 pages
https://doi.org/10.1155/2022/3274672

Research Article

Effect of Pin Geometry and Orientation on Friction and Wear Behavior of Nickel-Coated EN8 Steel Pin and Al6061 Alloy Disc Pair

Shiv Pratap Singh Yadav,[1] **Avinash Lakshmikanthan**,[1] **Siddappa Ranganath**,[2] **Manjunath Patel Gowdru Chandrashekarappa**,[3] **Praveena Bindiganavile Anand**,[1] **Vijay Kumar Shankar**,[1] **and Muralidhar Avvari**[4]

[1]*Department of Mechanical Engineering, Nitte Meenakshi Institute of Technology, Bangalore 560064, India*
[2]*Department of Mechanical Engineering, University Visvesvaraya College of Engineering, Bangalore 560001, India*
[3]*Department of Mechanical Engineering, PES Institute of Technology and Management, Shivamogga 577204, Visvesvaraya Technological University, Belagavi, India*
[4]*Faculty of Mechanical Engineering, Arba Minch Institute of Technology, Arba Minch University, Arba Minch, Ethiopia*

Correspondence should be addressed to Muralidhar Avvari; muralidhar.avvari@amu.edu.et

Received 1 November 2021; Revised 3 December 2021; Accepted 9 December 2021; Published 3 January 2022

Academic Editor: JT Winowlin Jappes

Most mechanical systems (in particular, gear transmission system) undergo relative motion which results in increased friction phenomenon (friction coefficient, stresses, and wear rate) and thereby results in loss of efficiency. Mechanical parts undergo relative motion in different geometry configurations and orientations that induce a different state of stress as a result of friction. Till date, attempts are being made to minimize the friction with full sphere pin geometry configuration. The present work focused to reduce the frictional and wear rate, and experiments are conducted with tribo-pairs. i.e., nickel-coated pin surface slide against Al6061 alloy disc. The friction studies are carried out at different loads and geometries of pin surfaces (sphere and hemisphere configured at different orientations such as full sphere and hemisphere configured at 0°, 45°, and 90°) to induce different stress states with reference to sliding directions. Change in the geometry of EN8 pin material and their orientation with reference to sliding direction resulted in a different state of stress. The resulting stress levels were examined under the scanning electron microscope, which revealed the mechanisms of adhesion, abrasion, and extrusion. At a lower magnitude of orientation and load, the extent of asperity breaking lessens and material removal from pin surface decreases. Abrasion wear mechanism was observed corresponding to full sphere configuration on Al 6061 disc, whereas adhesive wear mechanisms are seen with hemisphere pins. The amount of aluminum transfer on pin surface with a hemisphere pin is comparatively more than that of full sphere configuration. At a lower magnitude of state of stress, the mechanism of sliding was dominated by the adhesion effect. At a higher level of state of stress, the mechanism of sliding was dominated by abrasion and extrusion.

1. Introduction

Interface quality in moving parts is of practical significance to ensure proper function in the mechanical system [1, 2]. The drag and frictional forces are minimized due to their longitudinal ribs of shark, and tree frogs grip even on the smooth surface at wet environment due to their surface features (hexagonal cell separated by gaps observed in microstructure) [3, 4]. These observations ensure the study of surface properties, and their design for better performance in moving parts is of industrial relevance [5, 6].

Al alloys are extensively used in many industrial and household applications [7, 8]. Owing to excellent properties (high corrosion rate, good formability, and mechanical

properties) [9], Al 6061 finds major applications in automotive and marine applications [10]. Several attempts are being made to widespread the applications of Al6061 alloy by improving wear resistance with the addition of reinforcement materials [9–11]. The effect of reinforcement to Al6061 affects the machinability and formability and needs significant attention to bring back to optimal functioning conditions [12, 13]. Experimental study reveals that Al6061 composites exhibited better mechanical (tensile strength) and tribological (wear resistance) properties over Al7075 (high strength and high toughness) composites [10, 14]. Attempts are being made to enhance the tribological characteristics of two forge, and customary gear materials are evaluated [15]. Tests are conducted to examine the performance (friction coefficient, friction force, and wear rate) of planetary gear transmission (made of EN 24)-based CNC bending machine [16]. The tribological characteristic examination was performed on the pin-on-disc test rig against the different shaft materials (EN8 and EN24) with Al 6061 alloy under dry and wet conditions (SAE 20W50) [17]. The minimum coefficient of friction was observed with EN8-Al6061 tribo-pair [18]. It was observed that different geometric configuration (i.e., pin geometry: sphere-sphere, sphere-plane, block on ring, and piston ring-cylinder liner) induces different tribological characteristics (i.e., friction coefficient and wear rate) [18, 19]. Therefore, EN8-Al6061 tribo-pairs possess better tribological properties and require in-depth analysis (in terms of the state of stresses and friction developed, plastic deformation, and so on) at the different geometric configurations for further enhancement and widespread use of applications in industries.

A frictional phenomenon in moving parts brings loss in efficiency of the machine [20]. For example, spur gear efficiency was significantly affected by different frictional coefficients, load, velocity, and tooth profile [21]. Frictional parts subjected to periodic loading result in wear out of parts that causes increased clearances and losses of dimensional stability [22]. To minimize the frictional effects among moving parts, a series of experiments are conducted by distinguished researchers with material pairs, which are unlubricated, lubricated, and coatings [23, 24]. These techniques are basically employed to alter the displacement and velocity discontinuity across the contacting material pair [25, 26]. Therefore, significant attention is thus required to know the state of stress developed on sliding phenomenon for different tribo-pairs. The state of stress either a uniform or nonuniform is dependent on contacting surfaces (i.e., smooth surface results in steady state, whereas rough surface could result in the nonuniform state of stress) and load transfer between the mating element pairs [27]. It was confirmed that studying the different state of stress as a result of mating pairs are of practical significance. In spur gear applications, increased contact stresses are attributed to excessive load, which alter the gear tooth profile that causes wear on gear tooth [28, 29]. The contact stress can be minimized by altering the geometric parameters [30]. Excess wear on the tooth profile results in noise and vibration, which in turn reduces the efficiency [31, 32]. These phenomena are more common in mechanical transmission applications [28]. The effect of geometric parameters (gauge, gauge deficiency, cross-level, and longitudinal slope) on the wear phenomenon (lateral or vertical) of railway track was investigated [33]. It was observed that minimized wear with the right choice of geometric parametric conditions resulted in increased ride performance at reduced maintenance cost [34]. Creating artificial textures on the geometry of the cutting tools could help to minimize friction and wear [35]. These textures could help for better lubrication during the cutting phenomenon, thereby enhances the tool life and reduces workpiece surface roughness and power consumptions [20, 36]. Microtextures in the form of grooves, circle, rectangle, and hemisphere reduce the cutting temperature, friction, and wear that could enhance the tool life [37, 38]. The effect of pin geometries (flat and spherical) on the wear rate of low carbon steel material was investigated [39]. The results showed that the wear rate that corresponds to a flat pin is more than that of a spherical pin for a low load, whereas at higher loads, spherical pin quickly wears out. It was ascertained from the above literature review that changes in geometric parameters introduce different state of stress and help to control friction and wear. Therefore, the study of wear and friction phenomena as a result of geometric parameters and their orientations is of relative significance.

Coatings applied to substrate materials tend to improve the surface characteristics without affecting the properties of the parent material [40]. The application of coatings improves the hardness and surface integrity and reduces friction, wear, and corrosion [41–44]. Experiments are performed with EN8 carbon steel mating pair with ductile material Al6061 to know the wear phenomenon [45]. The magnetron deposition method was employed to coat aluminum oxide (Al_2O_3) on the aluminum substrate [46]. Compared to aluminum substrate, the coated samples resulted in reduced friction coefficient with enhanced strength and hardness were obtained. The friction and wear behaviors of hot-dip Al-Si and electroplated Zn-Ni alloy-coated steel blanks were investigated [47]. The coated Zn-Ni alloy resulted in better wear resistance at a reduced friction coefficient. The physical vapor deposition (PVD) technique was applied to coat the iron (Fe) nanoparticles on the flat surface of the pin on EN8 pin material, and the results are tested at room- and high-temperature applications [48]. The hard oxide layers are formed after sliding against pin material, which could help to sustain higher loads at elevated temperatures. Experiments are performed with Ni-P/bio-composite coating applied on EN 8 steel, which was subjected to friction and wear studies [49]. The coated samples resulted in a lower friction coefficient and wear rate than bare substrate material. The Mo-Ni-Cr coatings are applied on super-duplex stainless steel that resulted in better wear resistance and higher hardness than uncoated substrate material [43]. Nickel coatings are applied to H13 steel with the laser cladding technique that resulted in enhanced wear resistance and thermal fatigue characteristics [50]. The resistance to wear and corrosion, ductility, and microstructure characteristics are improved with nickel-based coatings [51, 52]. Nickel coatings find potential applications in

biomedical implants and automotive parts [53, 54]. Although coating technology improves the surface properties, the selection of the right choice of coating methods is often difficult as each technique possesses its own advantages and limitations. Electroplating is treated as a cost-effective technique compared to chemical vapor deposition and sputtering [55, 56]. In addition, electroplating coats materials in a single processing step (with faster, repeatable, control over the thickness of coating deposits and offers coating over a large surface area), which do not require costly equipment, materials, and nonhazardous method to deposit material on the substrates [57, 58]. There exists a significant scope to study the impact of electrodeposited nickel coatings on the substrate material for automotive applications. Most of the parts (prosthetic joint, crankshaft, connecting rod, brake pads, steering, chassis, axle housing, etc.) undergo either an individual or in the combination of sliding, reciprocating, and rotary actions [59–61]. Furthermore, tool wear occurred on die surface possessing sharp edges may not yield appropriate results with spherical or flat pin surfaces sliding against discs [39]. It was confirmed from the above literature review that applications of coatings increase the wear resistance. The said applications undergo wear with a different state of stress based on their contact movements and edge effects. Furthermore, not much research efforts have been made to examine worn surface morphology with different pin geometric configurations at different angles and applied loads to detail the insights of surface morphologies (plastic deformation and wear mechanism, i.e., adhesion, abrasion, and extrusion) relationship with friction and wear phenomenon.

To date, no studies have yet reported to study the field condition, which is arbitrary in terms of the state of stress concern. In this study, a cost-effective electrodeposited coating technique (widely employed with a growth rate of 15% per annum compared to other methods) [62] was used to apply nickel coating on the EN 8 steel pin. Nickel coatings are selected based on their properties, wide range of applications, and ability to withstand reduced wear loss both in oxidizing and nonoxidizing environments. The geometric parameters (spherical and hemispherical) of pin tip surface oriented at different angles are investigated to know the wear behavior and state of stress induced. Therefore, this study gives detailed insight into a different state of stress developed, friction induced, worn-surface morphologies (in terms of plastic deformation, abrasion, abrasive, and extrusion), and wear rate caused by different geometries and angle of orientation of pin surfaces with and without coatings.

2. Materials and Methods

EN 8 steel used in many mechanical parts due to better strength and toughness characteristics resulted in distinguished applications (connecting rod, spindles, axles, and so on) of automotive parts [63, 64]. Al 6061 alloy is used in commercial engineering and automotive applications due to better mechanical properties and ductility [9, 65]. The chemical composition of Al 6061 alloy disc and EN8 steel pin is presented in Table 1.

2.1. Electrodeposition Coatings. Nickel coatings based on electrodeposition technique were applied on the substrate material, i.e., EN8 steel. The dimensions of the pin specimens were equal to 9 mm × 35 mm (diameter and height), subjected to a nickel sulfate bath solution for coating applications as depicted in Figure 1. Prior to coating applications, the pins are cleaned (to remove the organic matter, present if any) after immersing in a dilute HCL acid bath solution. This process is referred to as the pickling process. After the acid pickling process, the pins are dipped in dilute sulfuric acid so as to improve the microroughness. This could help in better adhesion characteristics of coating on the substrate material. Note that, nickel coating was carried out by holding the pin as cathode and pure nickel as anode material in nickel sulfate solutions. The thickness of the coatings is about 100 μm and is decided after adjusting the duration of coating.

Pure nickel was selected to coat the substrate EN8 material due to their distinguished properties such as low friction and higher hardness with reduced wear and corrosion resistance properties [62]. Nickel electrodeposits are carried out, wherein nickel ion concentrations are varied subjected to 50–250 g/L, after maintaining Na_2SO_4 and boric acid fixed at 80 g/L and 10 g/L in the bath solution. It was observed that the bright deposits (without burnt) are attributed that correspond to the current density maintained equal to 3 Adm^{-2}. Note that during experimentation, the bath solution was maintained fixed that correspond to the potential of hydrogen equal to 3. Prior to electrodeposits, the solutions are subjected to agitation (say 500 rpm) for 24 hours at room temperature. From trial experimentations, it was clear that there is no presence of burnt appearance and uncoated regions when the pH value was maintained equal to 3. DC power source was used, and the depositions are carried out on substrate at the stagnant condition of bath solution. Schematic representation of electrodeposition technique used for coating nickel on EN8 substrate material is presented in Figures 2 and 3. Theoretically, the coating thickness was determined according to equations derived from the practical experiments.

$$\text{Thickness of coating} = \frac{\text{mass of deposit}}{\text{cross sectional area} \times \text{density of coating material}}. \quad (1)$$

Table 1: Chemical composition of EN8 steel and Al6061 alloy.

EN8 material	C	Si	Mn	Cr	Mo	Ni	P	S	Fe
wt. (%)	0.45	0.19	0.79	0.007	0.002	0.009	0.026	0.015	Balance
Al 6061 alloy	Mg	Si	Fe	Ca	Cu	Mn	Zn	Ti	Al
wt. (%)	0.92	0.6	0.33	0.20	0.18	0.06	0.03	0.02	Balance

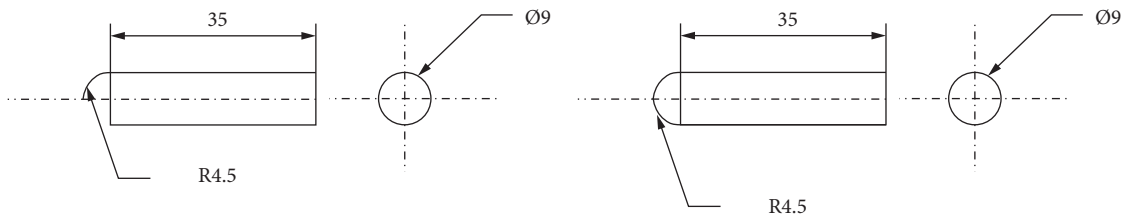

(a) (b)

Figure 1: Tipped EN8 pin surface with different configurations: (a) half-spherical shape and (b) spherical shape (all dimensions in mm).

(a) (b)

(c)

Figure 2: Nickel coating of EN8 pin. (a) Specimen preparation, (b) holding of specimens, and (c) nickel sulfate solution.

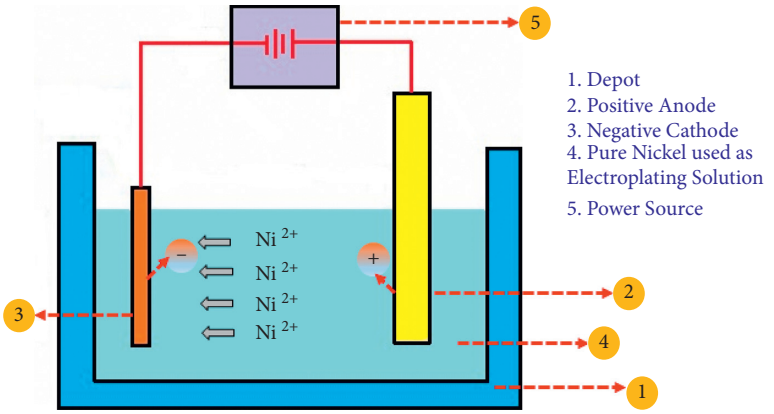

Figure 3: Schematic representation of electrodeposition coating.

2.1.1. XRD Characterization of Pin and Disc Materials. The XRD patterns of Al6061 are shown in Figure 4(a). The Al6061 XRD data show strong peaks at $2\theta = \sim 38.13^{\circ}$, $\sim 44.37^{\circ}$, followed by weaker peaks at $\sim 64.74^{\circ}$ and $\sim 77.88^{\circ}$, and $\sim 82.11^{\circ}$ due to the inherent Al content [66]. For Al 6061, the XRD pattern peak intensity is matched with JCPDS file card number 96-901-2004. In the case of Figure 4(b), i.e., EN8 steel pin (Peak 1), XRD data reveal sharp peaks at $2\theta = \sim 44.70^{\circ}$. Also, at $2\theta = \sim 65.09^{\circ}$ and $\sim 82.45^{\circ}$ dimmer peaks were detected owing to the intrinsic Fe content [66]. For EN8 steel pin, the XRD pattern peak intensity is matched with JCPDS file card number 96-900-6596. In the case of Figure 4(b), i.e., EN8 steel pin—Ni coated (Peak 2), the XRD data reveal sharp peaks at $2\theta = \sim 44.20^{\circ}$. The XRD pattern peak intensity of Ni-coated EN8 Pin is matched with JCPDS file card number no. 96-900-0658 and 96-901-2996. Similarly, at $2\theta = \sim 64.97^{\circ}$ and $\sim 82.28^{\circ}$ dimmer peaks were detected owing to the intrinsic Fe content. Also, the cause of a high broad peak at $\sim 44.20^{\circ}$ may be due to Ni-P coating [67, 68].

2.2. Experimental Details. The kinematic pair is treated as the building block in any mechanical system. The aluminum alloys are lightweight and possess excellent aesthetic qualities in any environment for a prolonged duration. Hot and cold extrusions are treated as the secondary route for processing aluminum parts. Tribo-phenomenon (i.e., mechanical interaction among stock and die) is of practical significance, as it decides the quality of parts. In the efforts of this research, understanding the tribo-phenomenon between die and aluminum stock is proposed to conduct laboratory experiments using a pin-on-disc test rig. The Al 6061 disc was used to simulate the stock in extrusion equipment. Electrodeposition of nickel material was performed to coat EN8 steel pin to a thickness of 100 μm.

The spherical (half and full) pin surface held at different angles against the rotating Al6061 disc could help to alter changes in the state of stress. The mating pair element in the disc form was precipitate hardened Al6061 alloy. Turning followed by facing operations ensures the dimensions of pin specimen possessing diameter and height equal to 9 and 35 mm, respectively. During experimentation (before and after), the pin and disc surfaces are ultrasonically cleaned with acetone. Figure 5 shows the pin-on-disc wear test rig, wherein the nickel-coated pin surfaces are subjected to three test loads (0.5, 3, and 5 kg or 4.9, 29.4, and 49.1 N). The wear tests are conducted at room temperature. Mechanical parts, namely, bearings, rotate smoothly at the speed of 100–250 rpm [69], wherein bearing supports gear parts, shafts, and so on. The test loads (0.5–5 kg) are selected in accordance with gear applications carried out earlier by authors [70, 71]. The wear parameters considered for examination on friction coefficient and wear rate are presented in Table 2. Three samples are separately prepared for each loading condition (0.5, 3, and 9 kg), and average values of three wear rate and coefficient of frictions are recorded to conduct analysis. The specimens are held on an aluminum disc, which is oriented at different configured stress state (full sphere and hemisphere configured at 0°, 45°, and 90°) with reference to sliding directions subjected to wear parameters (Figure 6). This could result in a different state of stress. Note that, after performing wear examination the surface topography of, namely, Al6061 and nickel-coated EN 8 steel is captured. SEM was performed to know the insight of wear mechanisms. The dimensions corresponding to Al 6061 disc are presented in Figure 7. Prior to wear examination, the pin and disc samples are examined for surface roughness and hardness. The surface roughness that corresponds to the uncoated pin, nickel-coated pin, and disc surface was maintained equal to 0.2 μm. The hardness values that correspond to uncoated pin, nickel-coated pin, and disc surfaces were found equal to 217.7 HV, 261.5 HV, and 98.1 HV.

3. Results and Discussion

The results of velocity discontinuity and state of stress caused by the sliding pair contact surfaces are discussed based on sliding mechanics. The EN8 pin surfaces coated with nickel for altering velocity discontinuity against the Al 6061 disc were also discussed. The state of stress altered by different pin tip-shaped surfaces (i.e., spherical and half-spherical) configured pin at different angles with reference to sliding direction. The state of stress as a result of different normal loads is discussed. Wear behavior and its mechanisms are examined with the help of scanning electron microscopic images.

3.1. Full Sphere Coated with Nickel Sliding against Al 6061 Disc. Figure 8 shows the coefficient of friction obtained for different loads with reference to time constraints. At 0.5 kg load, the friction coefficient increases from 0 to 0.18 for the duration of 5 seconds, and thereafter, a steady increase was observed till 110 seconds. Increased coefficient of friction with load might occur due to the plowing effect as a result of increased dislocation density, plastic deformation, and penetration depth [72]. Similarly, the coefficient of friction value tends to increase from 0 to ~0.5 till 10 seconds for 3 kg and 0 to ~0.56 till 8 seconds for 5 kg. The coefficient of friction remains at an almost steady state after crossing 10 seconds of duration. It was noted that at all loads the friction coefficient curves showed a similar trend, wherein the transient state was seen during the initial stage followed by a steady state (refer to Figure 8). The rate of increase in friction coefficient values was found to be of lesser magnitude after 10 seconds at all loads, compared to the time period of 0–5 seconds. This occurs because at the beginning of the experiments or sliding phenomenon, the soft disc (i.e., Al 6061 alloy) was plowed by the hard asperities of coating surfaces that resulted in the highest friction peaks. Similar observations are seen on friction performance of phosphate-coated brake materials [73]. A steady state with friction coefficient curves became flattened with the increased number of revolutions or time duration against sliding tests. As sliding continues, the hard asperities of coated pin surfaces slowly covered with accumulated transferred material (i.e., plowing mechanisms of

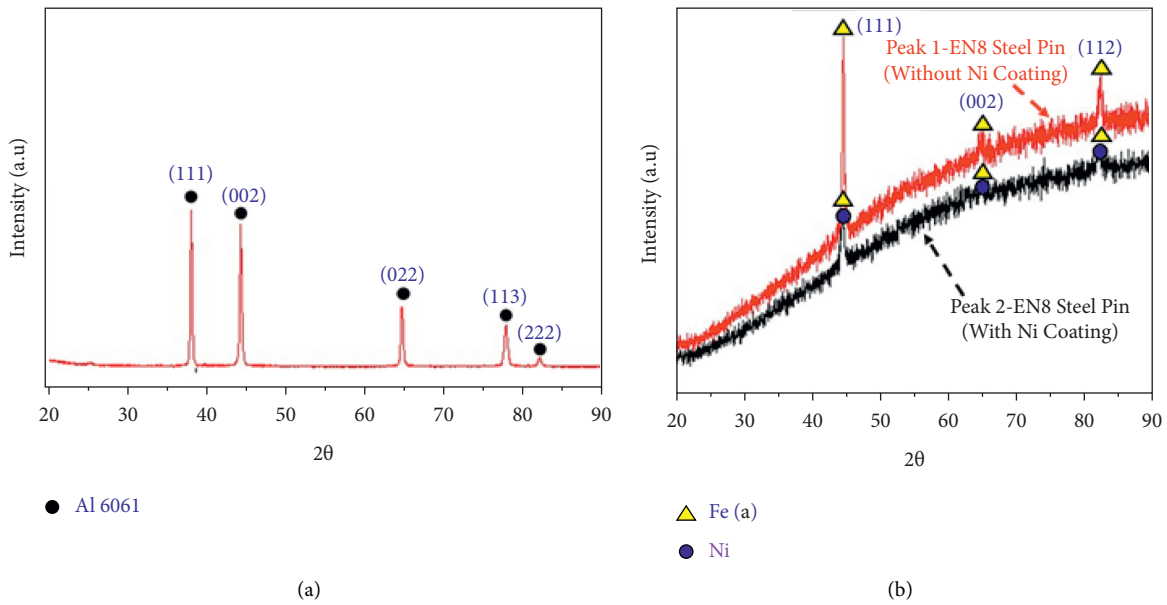

Figure 4: XRD analysis of (a) Al6061 disc and (b) EN8 steel pin (with and without Ni coating).

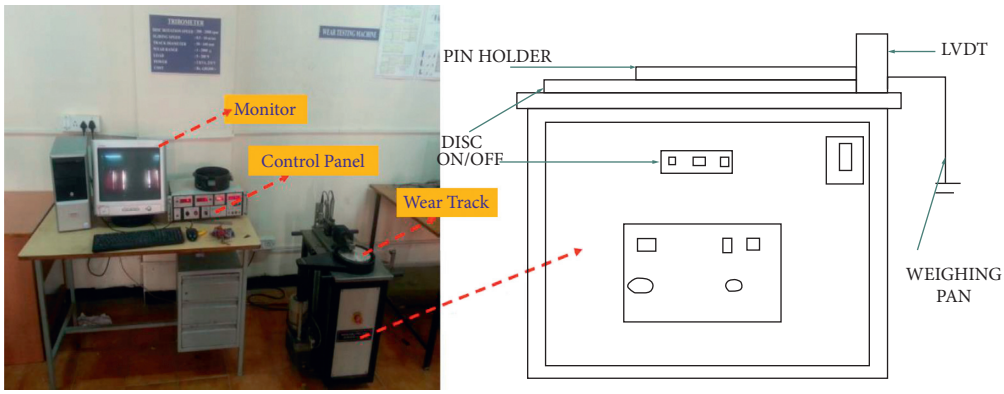

Figure 5: Schematic representations of pin-on-disc wear test rig with its line diagram.

Table 2: Experimental parameters for tribo-pairs: Al disc on EN8 steel pin (uncoated and coated).

S/No	Parameters	Aluminum disc on EN8 steel pin
1	Load (kg)	0.5, 3, and 5 kg
2	Track diameter (mm)	110 mm
3	Sliding time (seconds)	120 seconds
4	Speed (rpm)	250 rpm

hard asperities reduce, and in turn, friction coefficient becomes steady state), which was later deformed, and curves became flattened. The observations are similar to the friction behavior studies of titanium nickel coatings [74]. The average coefficient of friction tested at different loading conditions is presented in Table 3. The minimum and maximum friction coefficients were found equal to 0.3 for 0.5 kg and 0.48 for 3 kg loads, respectively. Interesting to note that, negligible change in friction coefficient values was attained after crossing the load from 3 kg to 5 kg. This is because more plastic deformation occurs at the sliding pairs as a result of compressive and shear forces [75].

3.2. Pin with Tip of the Hemisphere Coated with Nickel Configured 90° to the Sliding Directions against the Aluminum Disc. Figures 9(a)–9(c) show the variations of coefficient of friction for nickel-coated half-sphere configured at different orientations (0°, 45°, and 90°) sliding against Al6061 disc at different loads. For 0.5 kg load, the coefficient of friction rapidly increases from 0 to 0.33 up to 15 seconds at 90° orientation, 0 to 0.37 up to 35 seconds at 45° orientation, and 0 to 0.43 up to 8 seconds at 45° orientation, respectively. Similarly for 3 kg load, the coefficient of friction was found equal to 0.54 for 0°, 45°, and 90° orientations, respectively. However, for 5 kg load, the coefficient of friction steadily

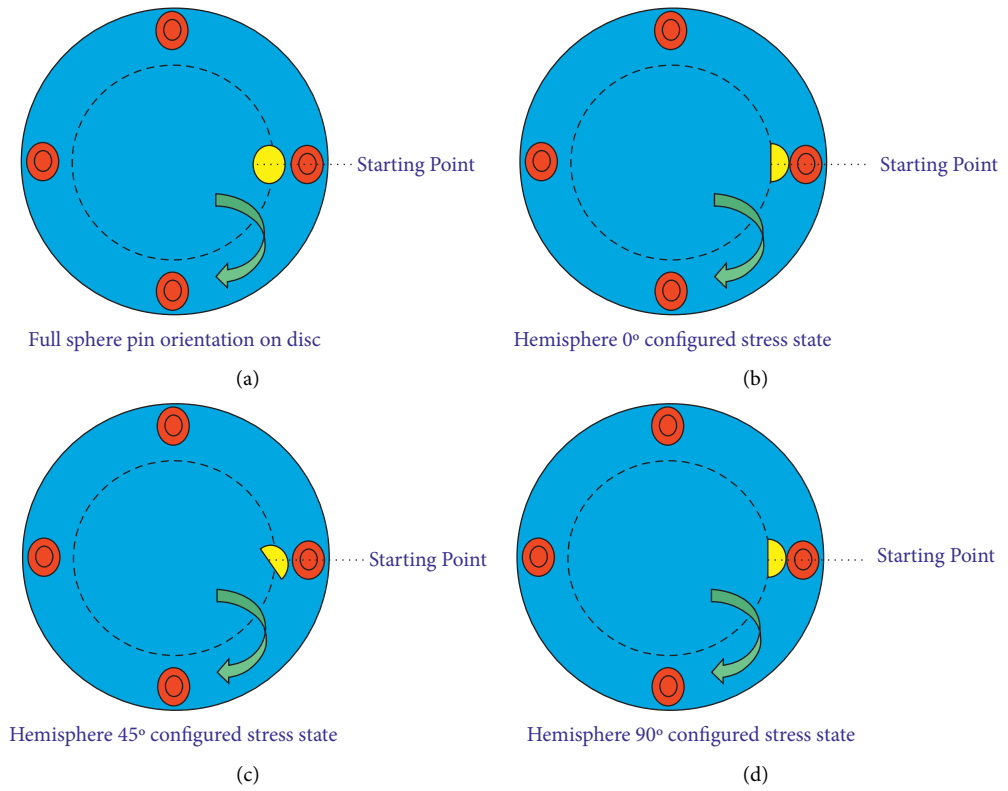

Figure 6: Schematic of aluminum disc with different orientations. (a) Full sphere pin orientation on disc; (b) hemisphere 0° configured stress state, (c) hemisphere 45° configured stress state, and (d) hemisphere 90° configured stress state.

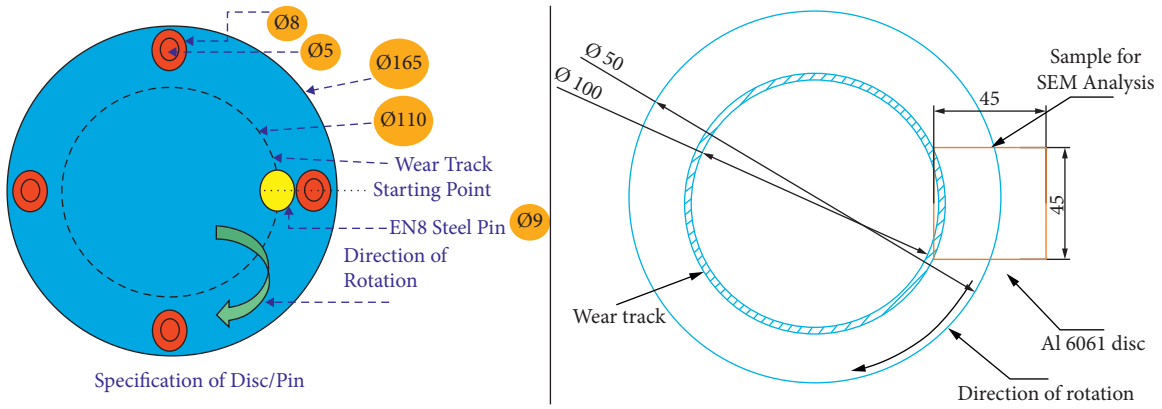

Figure 7: Schematic representations of Al6061disc.

increases to 0.6 for 0° and 45°, whereas 0.63 for 90° orientation of pin sample. It was clearly noted that comparatively stabilized friction curves were observed for 45° orientation than largest scatter (this occurrence might be due to stick-slip phenomenon) in friction values for 0° and 90°. It was clearly noticed from the friction curves that a rapid increase in friction at the initial stage of sliding due to soft aluminum disc was plowed by hard asperities of coatings. Thereafter, the surfaces are significantly altered such that original topographical orientation features (smooth surface ensures friction equalized to similar influenced values) possess minor variations showing that the friction curves remain flattened or steady for all orientations tested against different loads. Hard asperities of coatings tend to repeatedly indent the soft aluminum disc surfaces under stick-slip conditions, which results in increased sliding forces above the steady-state value during the beginning of experiments at all loads and orientations [76]. From Figures 9(a)–9(c), it was clear that the load at which both stick slips at start and amplitude oscillations are lower for 45° orientation than 0° and 90°. The average friction coefficients tested at different loads (0.5, 3, and 5 kg) against different pin configurations (0°, 45°, and 90°) are presented in Table 4. The coefficient of friction that increases with increasing load was clearly observed.

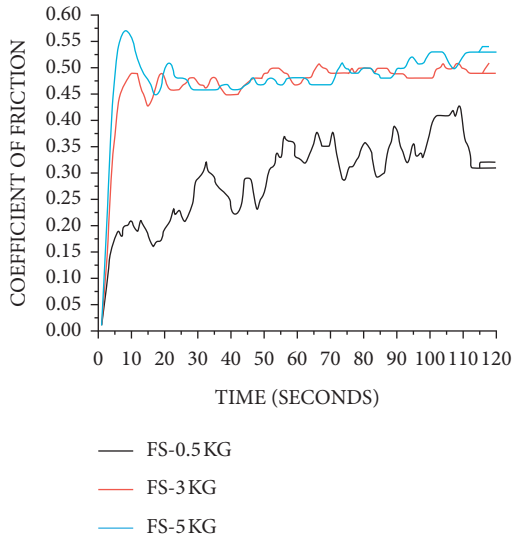

Figure 8: Coefficient of friction with sliding time at different normal loads.

Table 3: Average coefficient of friction for different load conditions.

Load (kg)	COF (μ) of sphere	
	With coating	Without coating
0.5	0.30 ± 0.031	0.55 ± 0.025
3.0	0.48 ± 0.035	0.68 ± 0.043
5.0	0.47 ± 0.038	0.70 ± 0.032

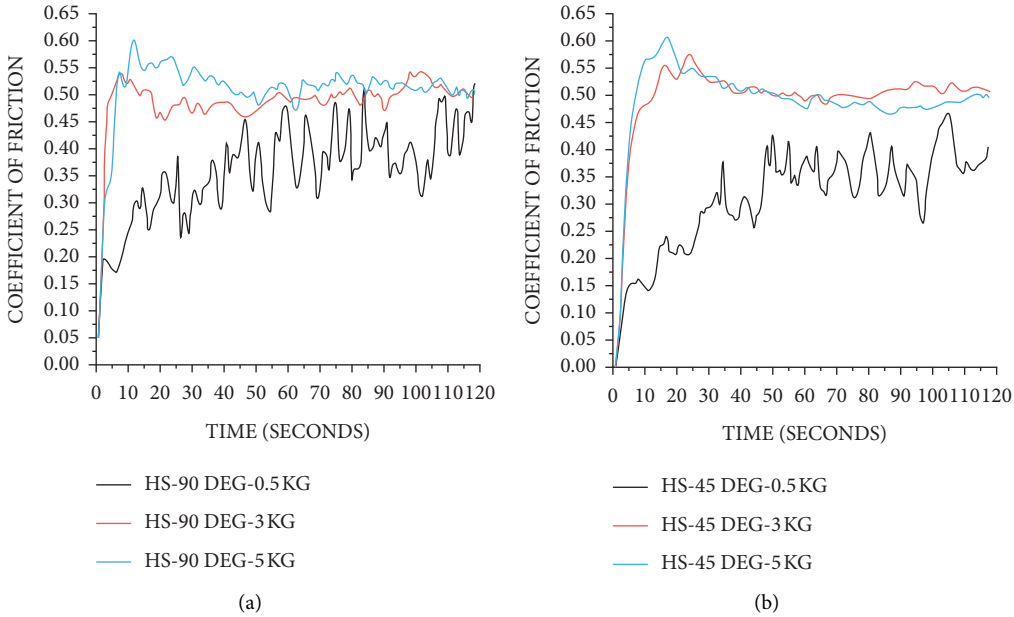

Figure 9: Continued.

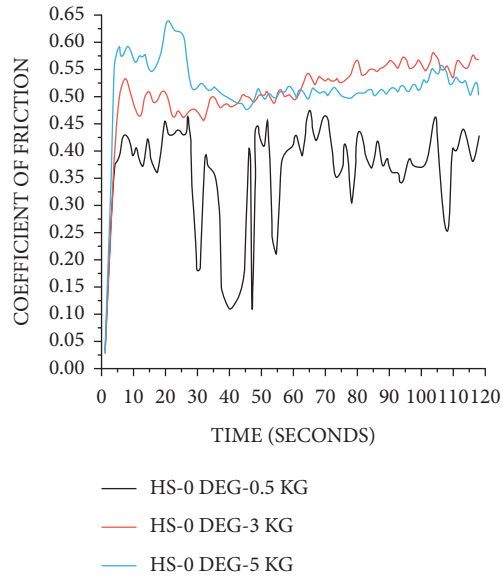

(c)

Figure 9: Coefficient of friction of nickel-coated half-sphere configured sliding against Al6061 disc with sliding time against different loads: (a) 90°, (b) 45°, and (c) 0°.

Table 4: Average coefficient of friction for different load conditions.

Load, kg	Coating samples: coefficient of friction, μ			Uncoated samples: coefficient of friction, μ		
	Pin configured at 90°	Pin configured at 45°	Pin configured at 0°	Pin configured at 90°	Pin configured at 45°	Pin configured at 0°
0.5	0.37 ± 0.025	0.33 ± 0.022	0.37 ± 0.028	0.61 ± 0.022	0.60 ± 0.012	0.62 ± 0.021
3.0	0.49 ± 0.045	0.51 ± 0.035	0.52 ± 0.031	0.68 ± 0.032	0.71 ± 0.025	0.71 ± 0.034
5.0	0.52 ± 0.052	0.50 ± 0.037	0.52 ± 0.028	0.71 ± 0.023	0.70 ± 0.017	0.72 ± 0.025

The surface topography orientation did not influence much on friction average friction coefficient for 0° and 90°, whereas comparatively lesser friction values were observed at 45° orientations. The plane strain conditions cause more amplitude of oscillations with higher frictions in the curves for 0° and 90° orientations. The reduced friction at 45° orientation is attributed to less continuous contact surface area. The behavior of pin geometry (full sphere and hemisphere) on frictional curves is presented in Figures 8 and 9. The mean values of coefficient of friction for spherical and hemispherical pins possess approximately similar magnitude values, with comparatively less friction for spherical pin surfaces (refer to Tables 3 and 4). The hemispherical pin friction curves showed that more fluctuations might be due to the damage that occurred at sliding or tribo-pairs, wherein the accumulated debris released from surface layers causes highly scattered variation in friction coefficients [77, 78]. However, full spherical pin surfaces are often smooth, which resulted in more stable friction. Similar observations are reported with different geometries of pin surfaces [79, 80]. Tables 3 and 4 clearly show that the nickel-coated pins resulted in a lesser coefficient of friction compared with uncoated or bare specimens. Increased hardness with nickel coating led to reducing the coefficient of friction values due to coating imparts, better oxide protection, and hot hardness properties. These observations are in good agreement with published literature [81].

3.3. Worn Surface Analysis of Al6061 Disc. Figure 10 depicts the wear surface morphology of Al6061 disc surfaces at different loads and orientations. From Figures 10(a)–10(h), the arrow mark represents sliding direction and the numbering 1, 2, and 3 represent flecks, slender abrasive furrows, and dense abrasive furrows, respectively. Figures 10(a)–10(b) show the SEM micrographs of track surface subjected to a load of 0.5 and 5 kg that correspond to the geometry of pin surface made of a full sphere. The track surface of a full sphere subjected to 5 kg load showed more abrasion than with 0.5 kg of load by pin material. Also, it is observed that a lesser extent of adhesions is observed on the track surfaces. Figures 10(c)–10(d) show the SEM micrographs and show the track of the hemispherical pin configured at 90° against sliding direction subjected to different loading conditions. Both figures showed more adhesion effects than that of abrasion. It can also be observed that the abrasion effects are comparatively larger than that obtained for Figure 9(a). Figure 9(c) shows more pronounced adhesion for 0.5 kg load compared to that obtained for 5 kg of load.

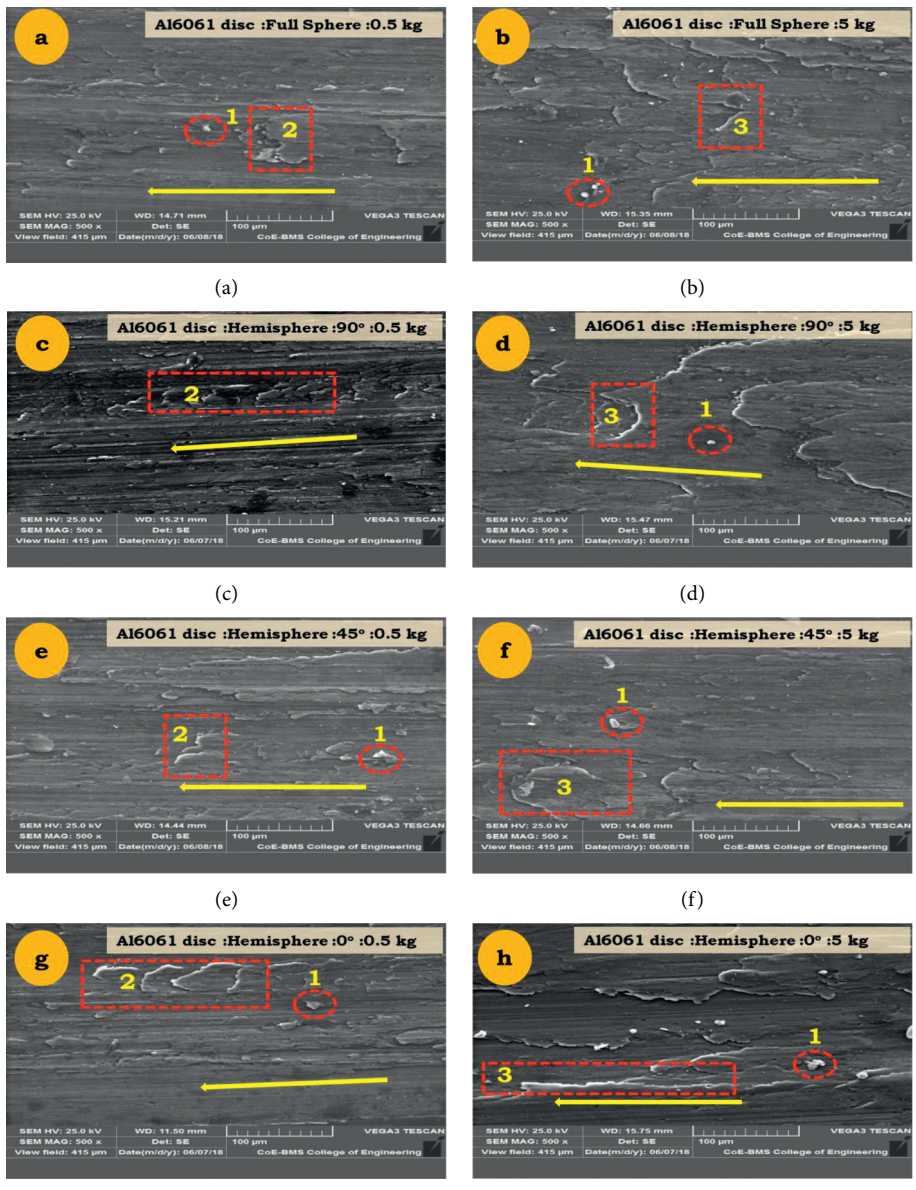

(a) (b) (c) (d) (e) (f) (g) (h)

Figure 10: SEM wear tracks of Al6061 disc surfaces for different load conditions and orientations.

Figure 10(d) clearly shows that there exists a larger extent of extrusion compared to the micrographs of Figures 10(a)–10(c). Figure 10(e) shows the track surface that corresponds to a pin configured to 45° against sliding direction subjected to different loads. The said figures clearly show that there is an extrusion phenomenon coupled with traces of abrasion. Figure 10(g) shows the small extent of abrasion, and the amount of extrusion was more pronounced for 5 kg normal load than that obtained for 0.5 kg against sliding direction. Under dry sliding conditions, there is a significant level of iron layer transfer from the EN8 steel pins to the surface of the aluminum disc plate. The amount of transferred layer was also found to increase load from 0.5 kg to 5 kg. Analogous remarks were made by quite a few researchers [76, 80, 82].

3.4. Worn Surface Analysis of the Nickel-Coated Pin. Figure 11 depicts the wear surface morphology of EN8 steel pin coated with nickel at different loads and orientations. From Figures 11(a)–11(h), the arrow mark represents cracks and the numbering 1, 2, and 3 represent slender abrasive furrows, material transfer area, and dense abrasive furrows, respectively. Figure 11(a) shows the SEM micrograph of pin surface for the full sphere at 0.5 kg load depicting the transfer of aluminum layer on the pin surface at a leading edge. Figure 11(b) presents the hemispherical pin configured to 90° that showed the aluminum layer transferred on the pin surface at the leading edge. Interesting to note that, the amount of aluminum transfer on the pin surface is comparatively more than that of the full sphere configuration seen in Figure 11(a). Similar observations were recorded for

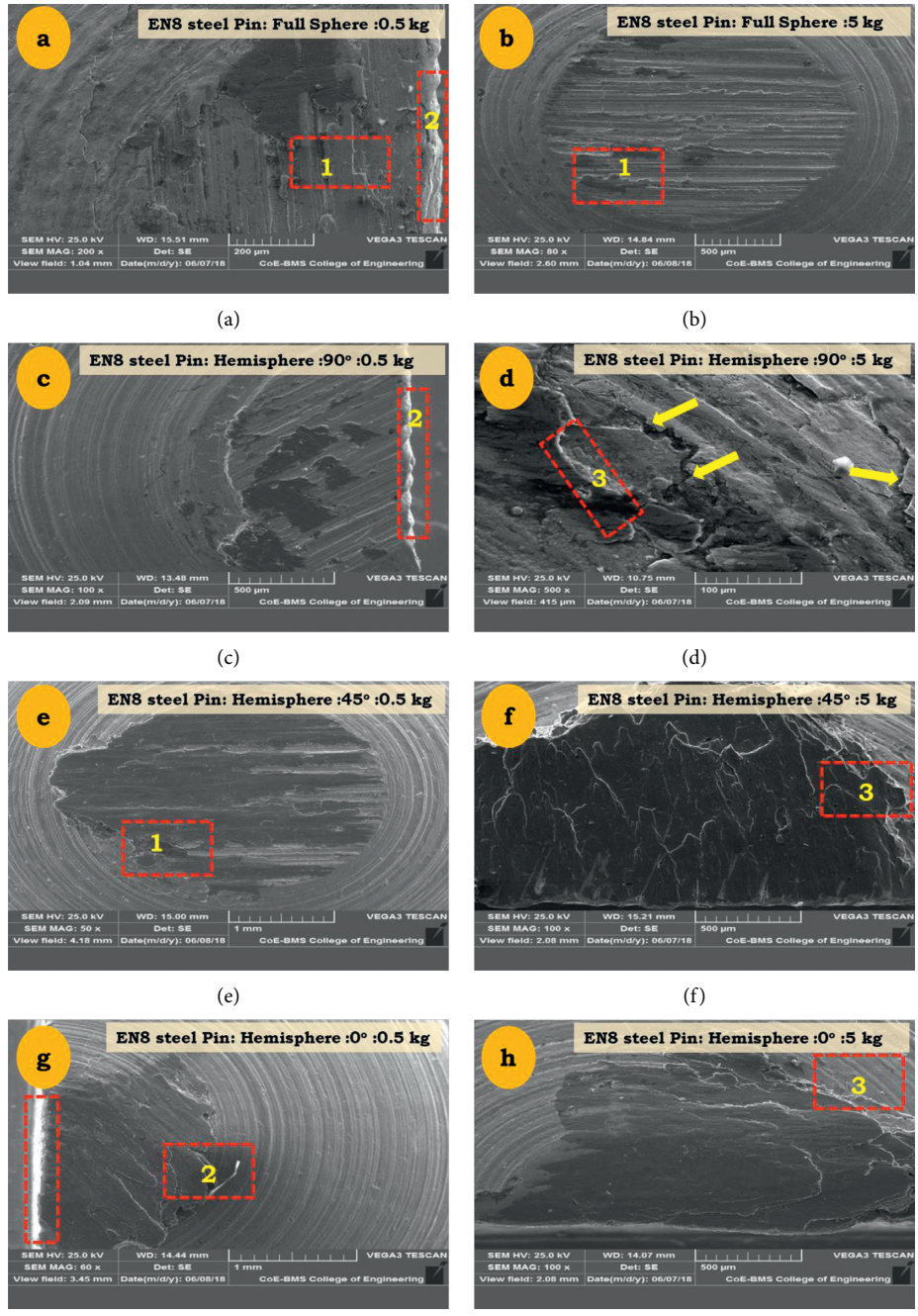

(a) (b) (c) (d) (e) (f) (g) (h)

Figure 11: SEM micrograph of nickel-coated pin surfaces for different load conditions and orientations.

a hemispherical pin configured to 45° and 0° as shown in Figures 11(c) and 11(d). Figures 11(e)–11(h) show the pin surface for all configurations at 5 kg load depicting aluminum transfer layer at the leading edge. Compared to 0.5 kg, the amount of aluminum transfer is quite large at 5 kg. Furthermore, as the steel pins slid across the aluminum plate, a few of the relatively weak asperities with poorer Al plate areas will indeed crack and then abide by the steel pin. The level of severity is such that these weaken the crack and relocate to the steel pin surface that is determined by oriented angle. While EN8 steel is slid tangential to the abrasion track rather than parallel to the sliding direction, the chances of breakdown of plate severities will surge. This is due to the asperities being aligned across the sliding direction when the oriented angle is 90° but along the sliding direction when the oriented angle is 0°. As the oriented angle and load are reduced, the extent of asperity breaking lessens, and thus, the extent of iron removal from the pin also decreases. Similar observations were made by several researchers [45, 76, 80, 83].

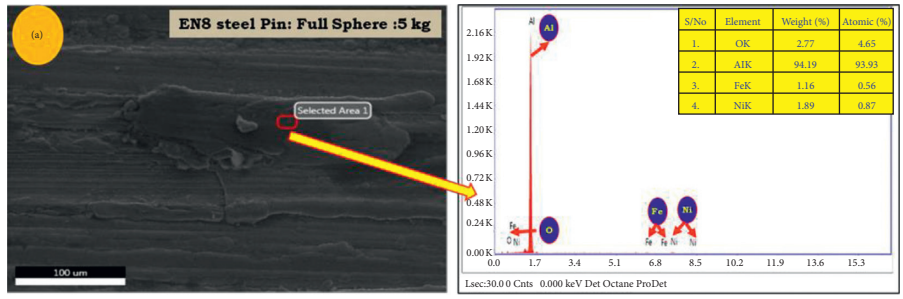

(a)

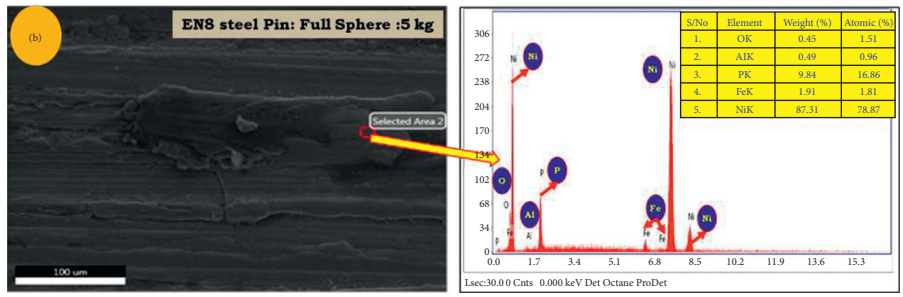

(b)

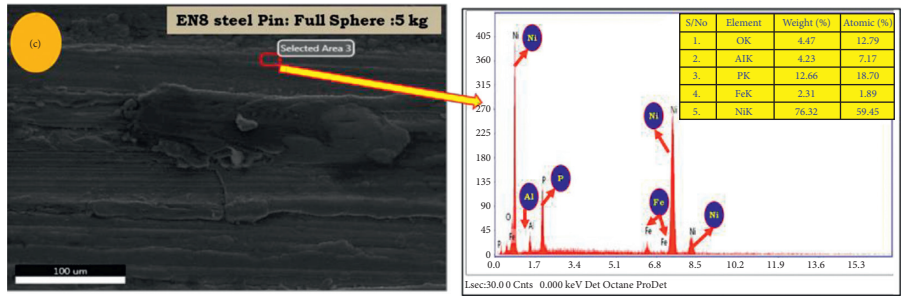

(c)

Figure 12: EDAX analysis of nickel-coated pin surfaces for different locations.

3.5. EDAX Analysis of the Nickel-Coated Pin. EDAX studies have been conducted for identifying elements present in worn surface and debris of nickel-coated spherical tipped pin surface at a load of 5 kg at different selected areas. The elemental analysis on transferred aluminum on pin surface was carried out at different locations and is shown in Figures 12(a)–12(c), respectively. From Figure 12(a), it was revealed that aluminum is 94.19 in weight percentage and the transfer layer is aluminum. Figure 12(b) reveals that nickel is 87.31 in weight percentage. The nickel coating is found to be intact. Figure 12(a) reveals that nickel is 76.32 in weight percentage. The nickel coating is found to be intact. From Figures 12(a)–12(c), the commonly observed elements were Al, Fe, Ni, and O. The occurrence of Fe implies that Fe has been transferred from the pin (EN8) to the disc surface, confirming the formation of an oxide layer on the disc, which protects the disc. The existence of thick oxides aids in the formation of wear protective layers.

4. Conclusions

The friction and wear behavior of tribo-pairs such as nickel-coated EN8 steel pin and Al6061 alloy disc was investigated at different loads and pin surface that configured to different geometries and orientations. The following conclusions that are drawn from this study are discussed in the following:

(1) Electrodeposition technique was applied to coat the nickel material onto the EN8 steel pin surfaces to a thickness of 100 μm. To induce a different state of stress, the geometry of pin surfaces is configured to full sphere and hemisphere with a different orientation (0°, 45°, and 90°) and load (0.5, 3, and 5 kg load).

(2) In full sphere configuration, the minimum and maximum friction coefficients were found equal to 0.3 for 0.5 kg, 0.48 for 3 kg loads, and 0.47 for 5 kg,

respectively. The plastic deformation that occurs at sliding pairs initiates at 3 kg load (as a result of compressive and shear forces), which resulted in a negligible change in friction coefficient values.

(3) The hemispherical pin friction curves showed that more fluctuations might be due to the damage that occurred at sliding or tribo-pairs, wherein the accumulated debris released from surface layers causes highly scattered variation in friction coefficients. However, full spherical pin surfaces are often smooth, which resulted in more stable friction.

(4) At higher load (say 5 kg), the abrasion and extrusion were more pronounced than 0.5 kg against sliding direction on the wear tracks of Al6061 disc surfaces.

(5) The amount of aluminum transfer on the hemisphere pin surface is comparatively more than that of full sphere configuration. As the oriented angle and load are reduced, the extent of asperity breaking lessens, and thus, the extent of iron removal from the pin also decreases.

(6) From COF vs. time plot, the coating studies are described by the transient state seen during the initial stage, followed by a steady state at all loads.

(7) Hard asperities of coatings tend to repeatedly indent the soft aluminum disc surfaces under stick-slip conditions, which results in increased sliding forces above the steady-state value during the beginning of experiments at all loads and orientations.

(8) From the wear surface morphology and surfaces at different loads and orientations, it is observed that a lesser extent of adhesion effects is observed than that of abrasion on the track surface effects [84].

Data Availability

Data used to support the findings of this study are available from the corresponding author upon request.

Conflicts of Interest

The authors declare that they have no conflicts of interest.

References

[1] C. J. Evans and J. B. Bryan, ""Structured," "textured" or "engineered" surfaces," *CIRP Annals*, vol. 48, no. 2, pp. 541–556, 1999.

[2] W. Huang, L. Jiang, C. Zhou, and X. Wang, "The lubricant retaining effect of micro-dimples on the sliding surface of PDMS," *Tribology International*, vol. 52, pp. 87–93, 2012.

[3] W. Federle, W. J. P. Barnes, W. Baumgartner, P. Drechsler, and J. M. Smith, "Wet but not slippery: boundary friction in tree frog adhesive toe pads," *Journal of The Royal Society Interface*, vol. 3, no. 10, pp. 689–697, 2006.

[4] D. W. Bechert, M. Bruse, W. Hage, and R. Meyer, "Fluid mechanics of biological surfaces and their technological application," *Naturwissenschaften*, vol. 87, no. 4, pp. 157–171, 2000.

[5] A. Parthasarathy, L. Avinash, K. N. Varun Kumar, B. Sajjan, and S. Varun, "Fabrication and characterization of Al-0.4% Si-0.5% Mg-SiCp using permanent mould casting technique," *Applied Mechanics and Materials*, vol. 867, pp. 34–40, 2017.

[6] L. Avinash, T. Ram Prabhu, A. Parthasarathy, K. N. Varun Kumar, and B. Sajjan, "Wear and mechanical behaviour of Hypo-eutectic Al-7% Si-0.5% Mg alloy (A357) reinforced with Al2O3 particles," *Applied Mechanics and Materials*, vol. 829, pp. 66–72, 2016.

[7] R. E. Melchers, "Time dependent development of aluminium pitting corrosion," *Advances in Materials Science and Engineering*, vol. 2015, no. 12, 10 pages, Article ID 215712, 2015.

[8] S. Jayaprakash, S. Siva Chandran, T. Sathish et al., "Effect of tool profile influence in dissimilar friction stir welding of aluminium alloys (AA5083 and AA7068)," *Advances in Materials Science and Engineering*, vol. 2021, Article ID 7387296, 7 pages, 2021.

[9] T. V. Christy, N. Murugan, and S. Kumar, "A comparative study on the microstructures and mechanical properties of Al 6061 alloy and the MMC Al 6061/TiB2/12p," *Journal of Minerals and Materials Characterization and Engineering*, vol. 9, no. 1, pp. 57–65, 2010.

[10] G. V. Kumar, C. S. P. Rao, N. Selvaraj, and M. S. Bhagyashekar, "Studies on Al6061-SiC and Al7075-Al2O3 metal matrix composites," *Journal of Minerals and Materials Characterization and Engineering*, vol. 9, no. 1, pp. 43–55, 2010.

[11] T. B. Rao and G. R. Ponugoti, "Characterization, prediction, and optimization of dry sliding wear behaviour of Al6061/WC composites," *Transactions of the Indian Institute of Metals*, vol. 74, no. 1, pp. 159–178, 2021.

[12] V. Anandakrishnan and A. Mahamani, "Investigations of flank wear, cutting force, and surface roughness in the machining of Al-6061–TiB 2 in situ metal matrix composites produced by flux-assisted synthesis," *International Journal of Advanced Manufacturing Technology*, vol. 55, no. 1, pp. 65–73, 2011.

[13] H. Karakoç, S. Karabulut, and R. Çıtak, "Study on mechanical and ballistic performances of boron carbide reinforced Al 6061 aluminum alloy produced by powder metallurgy," *Composites Part B: Engineering*, vol. 148, pp. 68–80, 2018.

[14] J. G. Kaufman, *Properties of Aluminum Alloys; Tensile, Creep, and Fatigue Data at High and Low Temperatures*, ASM International: Almere, Geauga, OH, USA, 2002.

[15] X. Li, M. Sosa, and U. Olofsson, "A pin-on-disc study of the tribology characteristics of sintered versus standard steel gear materials," *Wear*, vol. 340-341, pp. 31–40, 2015.

[16] N. H. Dhanvij, S. H. Gawande, and P. S. Gajjal, "Performance evaluation of EN24 for planetary gear transmission of CNC bending machine," *Journal of the Brazilian Society of Mechanical Sciences and Engineering*, vol. 42, pp. 1–17, 2020.

[17] M. Charool, M. Wani, M. Hanief, A. Chetani, and M. Rather, "Tribological characteristics of EN8 and EN24 steel against aluminium alloy 6061 under lubricated condition," *Advanced Materials Proceedings*, vol. 2, no. 7, pp. 445–449, 2017.

[18] W. K. Shafi and M. S. Charoo, "An overall review on the tribological, thermal and rheological properties of nano-lubricants," *Tribology: Materials, Surfaces & Interfaces*, vol. 15, no. 1, pp. 20–54, 2021.

[19] J. Takadoum, *Materials and Surface Engineering in Tribology*, Wiley, Hoboken, NJ, USA, 2013.

[20] C. Gachot, S. M. Hsu, H. L. Costa, and H. L. Costa, "A critical assessment of surface texturing for friction and wear improvement," *Wear*, vol. 372, pp. 21–41, 2017.

[21] D. Žeželj, A. Lončar, and K. Vučković, "Multi-objective spur gear pair optimization focused on volume and efficiency," *Mechanism and Machine Theory*, vol. 372-373, pp. 185–195, 2018.

[22] S. Baglioni, F. Cianetti, and L. Landi, "Influence of the addendum modification on spur gear efficiency," *Mechanism and Machine Theory*, vol. 49, pp. 216–233, 2012.

[23] L. Zemanová and P. Rudolf, "Flow inside the sidewall gaps of hydraulic machines: a review," *Energies*, vol. 13, no. 24, p. 6617, 2020.

[24] S. H. Adsul, K. R. C. Soma Raju, B. V. Sarada, S. H. Sonawane, and R. Subasri, "Evaluation of self-healing properties of inhibitor loaded nanoclay-based anticorrosive coatings on magnesium alloy AZ91D," *Journal of Magnesium and Alloys*, vol. 6, no. 3, pp. 299–308, 2018.

[25] S. Arulvel, A. Elayaperumal, and M. S. Jagatheeshwaran, "Controlling adhesive wear failure of nickel-phosphorus coating at high load condition using crab shell particle as reinforcement," *Engineering Failure Analysis*, vol. 90, pp. 310–323, 2018.

[26] T. He, Q. J. Wang, X. Zhang et al., "Visco-elastohydrodynamic lubrication of layered materials with imperfect layer-substrate interfaces," *International Journal of Mechanical Sciences*, vol. 189, Article ID 105993, 2020.

[27] V. Gurey, H. Shynkarenko, and I. Kuzio, "Mathematical model of the thermoelasticity of the surface layer of parts during discontinuous friction treatment," in *Design, Simulation, Manufacturing: The Innovation Exchange, Lecture Notes in Mechanical Engineering*, pp. 12–22, Springer International Publishing, Berlin, Germany, 2021.

[28] P. Põdra and S. Andersson, "Finite element analysis wear simulation of a conical spinning contact considering surface topography," *Wear*, vol. 224, no. 1, pp. 13–21, 1999.

[29] R. Prabhu Sekar and R. Sathishkumar, "Enhancement of wear resistance on normal contact ratio spur gear pairs through non-standard gears," *Wear*, vol. 380-381, pp. 228–239, 2017.

[30] W. J. Qin and C. Y. Guan, "An investigation of contact stresses and crack initiation in spur gears based on finite element dynamics analysis," *International Journal of Mechanical Sciences*, vol. 83, pp. 96–103, 2014.

[31] L. Ivanović, "Reduction of the maximum contact stresses by changing geometric parameters of the trochoidal gearing teeth profile," *Meccanica*, vol. 51, no. 9, pp. 2243–2257, 2016.

[32] J. H. Kuang and A. D. Lin, "The effect of tooth wear on the vibration spectrum of a spur gear pair," *Journal of Vibration and Acoustics*, vol. 123, no. 3, pp. 311–317, 2001.

[33] A. Lakshmikanthan, V. Mahesh, R. T. Prabhu, M. G. C. Patel, and S. Bontha, "Free vibration analysis of A357 alloy reinforced with dual particle size silicon carbide metal matrix composite plates using finite element method," *Archives of Foundry Engineering*, vol. 21, no. 1, pp. 101–112, 2021.

[34] J. Sadeghi and B. Akbari, "Field investigation on effects of railway track geometric parameters on rail wear," *Journal of Zhejiang University - Science*, vol. 7, no. 11, pp. 1846–1855, 2006.

[35] J. Sadeghi, "Sufficient experimental methods in investigation of dynamic behavior of track components and track system," in *Proceedings of the 7th International Conference on Mechanics of Systems*, pp. 71–79, University of Wollongong, Wollongong, Australia, June 2002.

[36] M. A. Khan and K. Gupta, "A study on machinability of nickel based superalloy using micro-textured tungsten carbide cutting tools," *Materials Research Express*, vol. 7, no. 1, Article ID 016537, 2020.

[37] M. Adam Khan and K. Gupta, "Optimization of machining parameters for material removal rate and machining time while cutting inconel 600 with tungsten carbide textured tools," in *Intelligent Manufacturing*, pp. 37–56, Springer, Berlin, Germany, 2021.

[38] A. Arslan, H. H. Masjuki, M. A. Kalam et al., "Surface texture manufacturing techniques and tribological effect of surface texturing on cutting tool performance: a review," *Critical Reviews in Solid State and Materials Sciences*, vol. 41, no. 6, pp. 447–481, 2016.

[39] S. Durairaj, J. Guo, A. Aramcharoen, and S. Castagne, "An experimental study into the effect of micro-textures on the performance of cutting tool," *International Journal of Advanced Manufacturing Technology*, vol. 98, no. 1, pp. 1011–1030, 2018.

[40] M. Mart'nez, A. Massetti, and H. Svoboda, "Effect of the pin geometry on the wear behavior of weld-deposited hardfacing," *Procedia Materials Science*, vol. 1, pp. 305–312, 2012.

[41] K. Holmberg and A. Matthews, *Coatings Tribology: Properties, Mechanisms, Techniques and Applications in Surface Engineering*, Elsevier, Amsterdam, Netherlands, 2009.

[42] C. M. P. Kumar, M. P. G. Chandrashekarappa, R. M. Kulkarni, D. Y. Pimenov, and K. Giasin, "The effect of Zn and Zn-WO3 composites nano-coatings deposition on hardness and corrosion resistance in steel substrate," *Materials*, vol. 14, no. 9, p. 2253, 2021.

[43] C. M. P. Kumar, A. Lakshmikanthan, M. P. G. Chandrashekarappa, D. Y. Pimenov, and K. Giasin, "Electrodeposition based preparation of Zn-Ni alloy and Zn-Ni-wc nano-composite coatings for corrosion-resistant applications," *Coatings*, vol. 11, no. 6, p. 712, 2021.

[44] G C Manjunath Patel, N B Pradeep, Girisha Lakhman Naik, H M Harsha, and A. K. Shettigar, "Experimental analysis and optimization of plasma spray parameters on microhardness and wear loss of Mo-Ni-Cr coated super duplex stainless steel," *Australian Journal of Mechanical Engineering*, vol. 2020, pp. 1–13, Article ID 1808760, 2020.

[45] H. A. Ching, D. Choudhury, M. J. Nine, and N. A. Abu Osman, "Effects of surface coating on reducing friction and wear of orthopaedic implants," *Science and Technology of Advanced Materials*, vol. 15, no. 1, Article ID 014402, 2014.

[46] S. Yadav, S. Ranganath, S. Sharieff, R. Suresh, and L. Avinash, "Investigations on the change in state of stress with respect to the sliding direction in dry sliding wear of hard elastic material with different geometry and orientation on ductile flat surface," *FME Transactions*, vol. 48, no. 3, pp. 716–723, 2020.

[47] A. D. Pogrebnyak, V. M. Beresnev, A. S. Kaverina et al., "Adhesive strength and physical, mechanical, and triboengineering properties of nano- and microstructural Al2O3 coatings," *Journal of Friction and Wear*, vol. 33, no. 3, pp. 195–202, 2012.

[48] G. Quercia, I. Grigorescu, H. Contreras, C. Di Rauso, and D. Gutierrez-Campos, "Friction and wear behavior of several hard materials," *International Journal of Refractory Metals and Hard Materials*, vol. 19, no. 4–6, pp. 359–369, 2001.

[49] J. C. Walker, S. R. Saranu, A. H. Kean, and R. J. K. Wood, "Fe nano-particle coatings for high temperature wear resistance," *Wear*, vol. 271, no. 9-10, pp. 2067–2079, 2011.

[50] M. S. Jagatheeshwaran, A. Elayaperumal, and S. Arulvel, "Wear characteristics of electroless NiP/bio-composite coatings on En8 steel," *Journal of Manufacturing Processes*, vol. 20, pp. 206–214, 2015.

[51] F. Yao and L. Fang, "Thermal stress cycle simulation in laser cladding process of Ni-based coating on H13 steel," *Coatings*, vol. 11, no. 3, p. 203, 2021.

[52] C. P. Paul, S. K. Mishra, P. Tiwari, and L. M. Kukreja, "Solid-particle erosion behaviour of WC/Ni composite clad layers with different contents of WC particles," *Optics & Laser Technology*, vol. 50, pp. 155–162, 2013.

[53] P. Farahmand, S. Liu, Z. Zhang, and R. Kovacevic, "Laser cladding assisted by induction heating of Ni-WC composite enhanced by nano-WC and La2O3," *Ceramics International*, vol. 40, no. 10, pp. 15421–15438, 2014.

[54] T. Ruthradevi, J. Akbar, G. Suresh Kumar et al., "Investigations on nickel ferrite embedded calcium phosphate nanoparticles for biomedical applications," *Journal of Alloys and Compounds*, vol. 695, pp. 3211–3219, 2017.

[55] A. Y. Cheng, H. H. Sheu, Y. M. Liu, K. H. Hou, P. Y. Hsieh, and M. D. Ger, "Effect of pretreatment process on the adhesion and corrosion resistance of nickel-boron coatings deposited on 8620H alloy steel," *International Journal of Electrochemical Science*, vol. 15, pp. 61–89, 2020.

[56] M. Schlesinger, *Modern Electroplating*, John Wiley & Sons, Hoboken, NJ, USA, 2011.

[57] N. Lotfi, M. Aliofkhazraei, H. Rahmani, and G. B. Darband, "Zinc-nickel alloy electrodeposition: characterization, properties, multilayers and composites," *Protection of Metals and Physical Chemistry of Surfaces*, vol. 54, no. 6, pp. 1102–1140, 2018.

[58] X. She, J. Wu, H. Xu et al., "Enhancing charge density and steering charge unidirectional flow in 2D non-metallic semiconductor-CNTs-metal coupled photocatalyst for solar energy conversion," *Applied Catalysis B: Environmental*, vol. 202, pp. 112–117, 2017.

[59] G. Barati Darband, M. Aliofkhazraei, S. Khorsand, S. Sokhanvar, and A. Kaboli, "Science and engineering of superhydrophobic surfaces: review of corrosion resistance, chemical and mechanical stability," *Arabian Journal of Chemistry*, vol. 13, no. 1, pp. 1763–1802, 2020.

[60] Z. Wang, B. Huang, H. Chen, C. Wang, J. Ma, and X. Zhao, "The effect of quenching and partitioning heat treatment on the wear resistance of ductile cast iron," *Journal of Materials Engineering and Performance*, vol. 29, no. 7, pp. 4370–4378, 2020.

[61] A. Borjali, K. Monson, and B. Raeymaekers, "Predicting the polyethylene wear rate in pin-on-disc experiments in the context of prosthetic hip implants: deriving a data-driven model using machine learning methods," *Tribology International*, vol. 133, pp. 101–110, 2019.

[62] B. Swain, S. Bhuyan, R. Behera, S. S. Mohapatra, and A. Behera, "Wear: a serious problem in industry," in *Tribology In Materials And Manufacturing-Wear, Friction And Lubrication*IntechOpen, London, UK, 2020.

[63] C. A. Loto, "Electroless nickel plating - a review," *Silicon*, vol. 8, no. 2, pp. 177–186, 2016.

[64] M. Ramesh, K. Marimuthu, P. Karuppusamy, and L. Rajeshkumar, "Microstructure and properties of YSZ-Al2O3 functional ceramic thermal barrier coatings for military applications," *Boletin de la Sociedad Espanola de Ceramica y Vidrio*, vol. 60, no. 6, 2021.

[65] D. Umapathi, A. Devaraju, C. Rathinasuriyan, and A. Raji, "Mechanical and tribological properties of electroless nickel phosphorous and nickel Phosphorous-Titanium nitride coating," *Materials Today Proceedings*, vol. 22, pp. 1038–1042, 2020.

[66] L. L. Natrayan, L. N. Singh, and M. S. Kumar, "An experimental investigation on mechanical behaviour of SiCp reinforced Al 6061 MMC using squeeze casting process," *International Journal of Mechanical and Production Engineering Research and Development*, vol. 7, no. 6, pp. 663–668, 2017.

[67] B. D. Cullity, *Elements of X-rays diffraction*, Addison-Wesley Publishing Co. Inc., Reading, MA, USA., 1956.

[68] S. Ankita and A. K. Singh, "Corrosion and wear resistance study of Ni-P and Ni-P-PTFE nanocomposite coatings," *Central European Journal of Engineering*, vol. 1, no. 3, pp. 234–243, 2011.

[69] J. N. Balaraju and K. S. Rajam, "Influence of particle size on the microstructure, hardness and corrosion resistance of electroless Ni–P–Al2O3 composite coatings," *Surface and Coatings Technology*, vol. 200, no. 12-13, pp. 3933–3941, 2006.

[70] A. Choudhury and N. Tandon, "Application of acoustic emission technique for the detection of defects in rolling element bearings," *Tribology International*, vol. 33, no. 1, pp. 39–45, 2000.

[71] A. Kumar, A. Patnaik, and I. K. Bhat, "Dry sliding wear behavior of Titanium metal powder filled aluminum alloy composites for gear application," *Applied Mechanics and Materials*, vol. 877, pp. 118–136, 2018.

[72] A. Kumar, A. Patnaik, and I. K. Bhat, "Tribology analysis of cobalt particulate filled Al 7075 alloy for gear materials: a comparative study," *Silicon*, vol. 11, no. 3, pp. 1295–1311, 2019.

[73] C. Gao and M. Liu, "Effects of normal load on the coefficient of friction by microscratch test of copper with a spherical indenter," *Tribology Letters*, vol. 67, no. 1, pp. 1–12, 2019.

[74] S. Fan, C. Yang, L. He, J. Deng, L. Zhang, and L. Cheng, "The effects of phosphate coating on friction performance of C/C and C/SiC brake materials," *Tribology International*, vol. 114, pp. 337–348, 2017.

[75] N. Thiyaneshwaran, C. P. Selvan, A. Lakshmikanthan, K. Sivaprasad, and B. Ravisankar, "Comparison based on specific strength and density of in-situ Ti/Al and Ti/Ni metal intermetallic laminates," *Journal of Materials Research and Technology*, vol. 14, pp. 1126–1136, 2021.

[76] J. Li, H. Liao, and C. Coddet, "Friction and wear behavior of flame-sprayed PEEK coatings," *Wear*, vol. 252, no. 9-10, pp. 824–831, 2002.

[77] P. L. Menezes and S. V. Kailas, "On the effect of surface texture on friction and transfer layer formation-a study using Al and steel pair," *Wear*, vol. 265, no. 11-12, pp. 1655–1669, 2008.

[78] P. J. Blau, "The significance and use of the friction coefficient," *Tribology International*, vol. 34, no. 9, pp. 585–591, 2001.

[79] O. Barrau, C. Boher, R. Gras, and F. Rezai-Aria, "Wear mechanisms and wear rate in a high temperature dry friction of AISI H11 tool steel: influence of debris circulation," *Wear*, vol. 263, no. 1-6, pp. 160–168, 2007.

[80] J. A. Williams, "Wear and wear particles-some fundamentals," *Tribology International*, vol. 38, no. 10, pp. 863–870, 2005.

[81] A. Lakshmikanthan, S. Bontha, M. Krishna, P. G. Koppad, and T. Ramprabhu, "Microstructure, mechanical and wear properties of the A357 composites reinforced with dual sized SiC particles," *Journal of Alloys and Compounds*, vol. 786, no. 25, pp. 570–580, 2019.

[82] S. Kumar, S. R. Maity, and L. Patnaik, "Friction and tribological behavior of bare nitrided, TiAlN and AlCrN coated MDC-K hot work tool steel," *Ceramics International*, vol. 46, no. 11, pp. 17280–17294, 2020.

[83] A. Lakshmikanthan, S. B. Udayagiri, P. G. Koppad, M. Gupta, K. Munishamaiah, and S. Bontha, "The effect of heat treatment on the mechanical and tribological properties of dual size SiC reinforced A357 matrix composites," *Journal of Materials Research and Technology*, vol. 9, no. 3, pp. 6434–6452, 2020.

[84] N. Vinayaka, A. Lakshmikanthan, G. C. M. Patel, and C. Pon, "Mechanical, microstructure and wear properties of Al 6113 fly ash reinforced composites: comparison of as-cast and heat-treated conditions," *Advances in Materials and Processing Technologies*, vol. 2021, Article ID 1927649, 2021.